A potent myeloid response is rapidly activated in the lungs of premature Rhesus macaques exposed to intra-uterine inflammation.

Courtney M. Jackson[1,2*], Martin Demmert[1,3*], Shibabrata Mukherjee[1], Travis Isaacs[1], Jerilyn Gray[4], Paranthaman Senthamaraikannan[4], Pietro Presicce[5], Kashish Chetal[6], Nathan Salomonis[6], Lisa A. Miller[7], Alan H. Jobe[4], Suhas G. Kallapur[5], William J. Zacharias[4,8], Ian P. Lewkowich[1], Hitesh Deshmukh[4], Claire A. Chougnet[1#]

1. Division of Immunobiology, Cincinnati Children's Hospital Research Foundation, Department of Pediatrics, University of Cincinnati College of Medicine, Cincinnati, Ohio, USA
2. Immunology Graduate Program, University of Cincinnati College of Medicine, Cincinnati, Ohio, USA
3. Department of Pediatrics, Institute for Systemic Inflammation Research, University of Lübeck, Lübeck, Germany
4. Division of Neonatology/Pulmonary Biology, The Perinatal Institute, Cincinnati Children's Hospital Research Foundation, Department of Pediatrics, University of Cincinnati College of Medicine, Cincinnati, Ohio, USA
5. Divisions of Neonatology and Developmental Biology, David Geffen School of Medicine at the University of California Los Angeles, Los Angeles, CA USA
6. Division of Biomedical Informatics, Cincinnati Children's Hospital Research Foundation, Department of Pediatrics, University of Cincinnati College of Medicine, Cincinnati, Ohio, USA
7. California National Primate Research Center, University of California Davis, Davis, CA, Department of Anatomy, Physiology, and Cell Biology, School of Veterinary Medicine, University of California Davis, Davis, CA USA
8. Division of Pulmonary and Critical Care Medicine, Department of Internal Medicine, University of Cincinnati, Ohio, USA

*Contributed equally.

#Corresponding author: Dr. Claire Chougnet, Division of Immunobiology, Cincinnati Children's Hospital Medical Center, MLC #7038, 3333 Burnet Avenue, Cincinnati, OH 45229-3039. E-mail address: Claire.Chougnet@cchmc.org, phone number: 513-636-8847, fax number: 513-636-5355

Abstract

Intrauterine inflammation/infection (IUI), which is present in up to 40% of premature births, leads to elevated levels of pro-inflammatory mediators and microbial products within the amniotic fluid, which come in close contact to fetal mucosae. Yet, knowledge on the fetal mucosal responses to IUI exposure remains limited. To address these questions, we used a non-human primate model of IUI, in which pregnant Rhesus macaques received intra-amniotic (IA) LPS, compared with IA saline.

We found that IA LPS exposure induced a robust and rapid inflammation of the fetal lung, but not the intestine. This inflammatory response was characterized by high levels of pro-inflammatory cytokines in the lung and the alveolar wash, and a potent myeloid cell response, dominated by neutrophils and monocytes/macrophages. scRNAseq analyses of fetal lungs showed that the infiltrating (neutrophils and inflammatory monocytes) and the resident (alveolar and interstitial macrophages) myeloid cells exhibited transcriptional profiles consistent with exposure to TLR ligands, as well as to cytokines, notably IL-1 and TNFα. However, blocking IL-1 signaling or TNFα, alone or simultaneously by administering inhibitors intra-amniotically and subcutaneously to the dam only partially blunted fetal lung inflammation.

Together, our novel data indicate that the fetal innate immune system can mount a rapid multi-factorial mucosal innate response to IUI, responding both to direct signaling by bacterial products and to indirect cytokine-mediated pathways of activation. These data thus provide more mechanistic insights into the association between IUI exposure and the post-natal lung morbidities of the premature infant.

57

Introduction

Intrauterine inflammation/infection (IUI) is present in 25-40% of premature births[1]. Inflammation of the placental membranes at the fetal-maternal interface, which is called chorioamnionitis (chorio)[2], leads to elevated levels of pro-inflammatory mediators and microbial products within the amniotic fluid [2-5]. Due to *in utero* aspiration/swallowing of the amniotic fluid [6,7], the mucosae of the developing fetus come in close contact with these mediators, which triggers an inflammatory response. Although such responses likely contribute to the increased incidence of post-natal pulmonary and intestinal morbidities associated with IUI exposure [8-10], knowledge about the cells and pathways involved in the fetal mucosal response remains very limited, due to the inability to collect tissue samples in preterm infants.

Fetal lung and intestinal inflammation have been described in IUI animal models (rodent, rabbits, pig, and sheep). Main features include high levels of pro-inflammatory cytokines and infiltration of immune cells, as well as damage to the lung and intestine [11-18]. However, the ontogeny of the immune system or the placenta structure are quite different in these species from those in humans. In contrast, non-human primates (NHP) are quite similar to humans in most biological aspects. Furthermore, many reagents developed against human antigens are cross-reactive allowing for in-depth analysis of the NHP fetal immune system[19-21]. Importantly, we have previously shown that intra-amniotic (IA) injection of LPS in pregnant Rhesus macaques leads to a type of inflammation that closely phenocopies severe human chorio [22,23]. Previous studies from ours and other groups have reported elevated levels of inflammatory cytokines in the lung of IUI-exposed rhesus macaque fetuses [24,23], but no in-depth analysis of mucosal immune

81 responses was performed in these studies. Our goal herein was thus to apply state-of-

82 the art technologies, such as single-cell RNAseq (scRNAseq), to obtain a comprehensive

83 view of the mucosal immune responses occurring in response to IUI.

84   Furthermore, this model allows us to evaluate the role inflammatory cytokines may

85 play in these responses. Among the cytokines elevated in the amniotic fluid and cord

86 blood in chorio, IL-1β and TNFα appear particularly important [4,25]. Indeed, both cytokines

87 are capable of inducing chorio, and neutrophil infiltration into the fetal lung of Rhesus

88 macaques when administered IA to pregnant dams [26,27]. In addition, IL-1β is involved in

89 many aspects of LPS-induced fetal inflammation [22,23,27-30]. We thus aimed at better

90 delineating their respective role, using the cross-reactive IL-1 receptor antagonist (IL-

91 1RA) and a blocking anti-TNF Ab (Adalimumab) given either individually, or in

92 combination.

93   Herein, we show that IA LPS leads to rapid and robust inflammation of the fetal

94 lung, but not of the fetal intestine. Notably, our analyses identified two main components,

95 i.e., the recruitment of innate myeloid cells into the fetal lung, and the activation of resident

96 lung myeloid cells. Although signaling by IL-1 and TNFα were identified as major

97 transcriptional signatures in responsive myeloid cells, their individual or combined

98 blockade only partially blunted fetal lung inflammation. Together, our novel data thus

99 indicate that the fetal innate immune system is capable of mounting a rapid multi-factorial

100 mucosal response to IUI, responding both to direct signaling by bacterial products such

101 as LPS, and to indirect cytokine-mediated pathways of activation.

102

Results

IA LPS induces robust inflammation in the fetal lung with a minimal response in the small intestine.

To model IUI, pregnant Rhesus macaques were given intra-amniotic (IA) injection of LPS or saline at approximately 80% gestation. Sixteen hours post IA injections, the fetuses were surgically removed, and tissues collected for analysis. All the animals included in the study are described in Table S1.

We first examined the histological changes in the fetal lung and small intestine. Compared to controls, lungs from 16hr IA LPS-exposed fetuses displayed signs of inflammation with cell infiltration into the lung interstitium and decreased alveolar space (Fig. 1A). Secondary alveoli septa formation also appeared diminished (Fig. 1A). In contrast, in the jejunum of exposed fetuses, the intestinal villi, lamina propria, or the underlying mucosal area exhibited no abnormalities (Fig. S1A). Because intestinal inflammation did not develop until 3 days after IUI in other models (pig[18] and sheep [12,17,31]), we analyzed jejunum sections taken 48 and 120hrs post IA LPS, and again, found only minimal changes compared to controls (Fig. S1A).

Along with histological evaluations, mRNA expression of inflammatory cytokines was measured in lung and jejunum at 16hrs post IA LPS. TNFα, IL-6, and IL-1β mRNA levels were greatly increased in the lung (>100-fold) of IA LPS-exposed fetuses along with increased detection of these cytokines in the alveolar wash (AW) (Fig. 1B, C). Other pro-inflammatory cytokines such as IL-8 and CCL2 were also increased (see Tables S2 and S3). In contrast, IL-10, a known anti-inflammatory molecule was only minimally increased

6

125 in the AW of LPS-exposed infants (Table S2). In agreement with the absence of

126 histological alterations in the jejunum, mRNA expression of inflammatory cytokines was

127 not significantly increased in this compartment (Fig. S1B). Thus, IA LPS induces a rapid

128 inflammatory response within the fetal lung but has minimal impact on the fetal small

129 intestine. Our in-depth analyses of fetal mucosal responses thus focused on the lung.

130

131 **IA LPS triggers a large infiltration of myeloid cells into the fetal lung.**

132 We next evaluated by scRNAseq the global transcriptional response of the lung in

133 response to IA LPS (animals and sequencing metrics are described in Table S4). These

134 analyses revealed distinct immune and non-immune cell populations in both control and

135 IA LPS-exposed animals (Fig. 2A, Table S5). As our focus was on immune responses,

136 subsequent analyses were performed on a subset of the whole dataset, containing only

137 the immune cell clusters. (Fig. 2B). Using established lineage marker genes (see Fig.

138 2C), we identified the robust accrual of neutrophilic and monocyte/macrophage

139 populations in the lung of IA LPS-exposed fetuses, compared to control animals (Fig. 2B).

140 As expected, they highly expressed the myeloid-associated CD88 gene (*C5AR1*, Fig.

141 2D). These findings were confirmed by flow cytometric analyses of lung cell suspensions

142 (see gating strategy in Fig. S2), which showed a trend toward a higher proportion of

143 CD45$^+$ hematopoietic cells, and, within this population, a significant increase in the

144 proportion of CD88$^+$ cells (Fig. 2E).

145 Due to the rapid response within the lung and the type of challenge used, another myeloid

146 population of interest were dendritic cells (DCs), as DC populations have been described

147   in the human fetal lung[32]. By flow cytometry, we readily identified myeloid dendritic cells

148   (mDCs) and plasmacytoid DCs (pDCs) in the lung, but their frequencies were unchanged

149   by IA LPS (Fig. S3). However, these DCs appeared activated in IA LPS-exposed fetuses,

150   as they both exhibited significantly increased HLA-DR levels (Fig. S3A-B).

151   In contrast to the brisk myeloid response, the frequency of B cells or different T cell

152   populations, including regulatory T cells, was not changed by IA LPS as seen by flow

153   cytometry and scRNAseq analyses (Fig. S4A-D). Additionally, analyses of differentially

154   expressed genes (DEGs) also uncovered relatively few changes (n=342) in these

155   populations between IA LPS and control animals (Fig S4B, S4D, Table S6).

156   Taken together, our data show that IA LPS rapidly affected fetal innate immune cell

157   populations   in   the   lung,   mainly   altering   myeloid   cells   (neutrophils,

158   monocytes/macrophages, DCs), while having little effect on the major lymphoid cell

159   subsets.

160

161   **IA LPS leads to the recruitment of inflammatory monocytes into the fetal lung and**

162   **activates the resident macrophages.**

163   scRNAseq analyses of the lungs of control fetuses revealed the presence of 2

164   macrophage populations (Fig. 3A), which we identified as alveolar and interstitial

165   macrophages (Fig. 3B and S5). In the lung of IA LPS-exposed fetuses, another population

166   of monocytes/macrophages with characteristics of inflammatory monocytes was also

167   present (Fig. 3A-B and Fig. S5).

168   Next, we identified DEGs in alveolar and interstitial macrophages of IA LPS exposed

169   lungs compared to controls. The majority of these DEGs were more highly expressed in

170   LPS than in controls (n=482/620 in alveolar macrophages and n=302/324 in interstitial

171   macrophages; Table S7, S8). Gene ontology (GO) enrichment analysis of these

172   upregulated genes revealed several biological processes, including activation of the TLR

173   signaling pathway, and response to cytokines, notably to IL-1 and TNF (Fig. 3C, Tables

174   S9 and S10 for full list of genes). Furthermore, genes associated with apoptotic signaling

175   and cell migration were particularly enriched (Fig. 3C). The fewer down-regulated genes

176   in the alveolar and interstitial macrophages of IA LPS lungs mainly included ribosomal

177   protein genes (Tables S6 and S7).

178   There was no inflammatory monocyte cluster in the control lungs, precluding DEG

179   analysis. However, single sample gene set enrichment analysis (ssGSEA) of this

180   population in the IA LPS-exposed lungs revealed a similar profile as that found in the

181   alveolar and interstitial macrophages from the same lungs. Indeed, there was an

182   enrichment of genes related to activation of the TLR, IL-1 and TNF signaling, as well as

183   cell migration and apoptosis (Fig. 3D, Table S11 for full list of genes expressed and

184   enrichment scores). All together, these data thus show that exposure to IUI strongly

185   affects fetal lung resident macrophages as well as rapidly inducing the afflux of activated,

186   inflammatory monocytes into the fetal lung.

187

188   **Recruited neutrophils into the fetal lung have a profile of activation suggesting**

189   **both direct LPS and indirect cytokine-mediated pathways of activation.**

9

190   Our data also showed a strong neutrophilic response in the fetal lung after IA LPS.

191   scRNAseq analyses identified *TNFAIP6* (TNF Alpha Induced Protein 6) expression as

192   one of the most specific markers for neutrophils (Fig. 4A and Fig. S6A). *S100A8* was

193   also found to be highly expressed in most neutrophils, although it was also present in the

194   monocyte/macrophage cluster (Fig. 4A). The cluster was further uniquely characterized

195   by the expression of neutrophil specific markers *AZU1*, *ITGAM*, *NCF2*. By IHC, we

196   confirmed the presence of multiple TNFAIP6⁺S100A8⁺ cells in the IA LPS fetal lungs,

197   which were not present in control lungs (Fig. 4B). These cells had neutrophilic

198   morphology, and they formed aggregates within alveolar spaces (Fig. 4B-C). We

199   confirmed these data by staining with CD68 and HLA-DR, as we had found that CD68 is

200   highly expressed in both fetal neutrophils and monocytes/macrophages, with only the

201   latter expressing HLA-DR. A significantly increased number of CD68⁺HLA-DR⁻ cells, with

202   a neutrophilic morphology, were found in the IA LPS-exposed lungs, also forming

203   aggregates (Fig. S6B). Furthermore, we found a significant number of neutrophils in the

204   AW of IA LPS exposed fetuses, whereas they were largely absent in the AW of control

205   fetuses [median 0.0 v. 106.3×10^6 cells/kg in control (n=18) and IA-LPS (n=13),

206   respectively, p<0.0001, Mann-Whitney test].

207   We next analyzed the transcriptomic program of the neutrophils recruited in the fetal lungs

208   by ssGSEA. These analyses revealed the enrichment of similar processes as those found

209   in monocytes/macrophages, notably migration, response to TLR, IL-1 and TNF, and

210   apoptosis (Fig.4D and Table S12 for full list of genes expressed and enrichment scores).

211   Interestingly, and in line with other studies[33,34], substantial transcriptional heterogeneity

212   could be seen within these recruited neutrophils. However, no distinct sub-clusters were

213   revealed by UMAP projection (Fig. 5A), suggesting different levels of maturation and/or

214   activation. We therefore applied pseudo-time analyses as implemented in Monocle3 to

215   characterize this heterogeneity. Genes that most determined the trajectory were

216   calculated with spatial autocorrelation analysis (Fig. S7). This analysis revealed that

217   cytokine and cytokine-response genes were particularly enriched close to the beginning

218   of the trajectory, whereas expression of other effector genes (e.g., *S100A8/9, CAMP,*

219   *MMP8*) was higher towards more advanced pseudo-time (Fig. 5, S7 and S8). Thus, the

220   recruited neutrophils into the fetal lung exhibit transcriptional programs revealing different

221   stages of activation, compatible with both direct activation by LPS and indirect cytokine-

222   mediated pathways.

223

224   **IL-1 and TNFα signaling are partially driving fetal lung inflammation.**

225   Knowing the role of IL-1 and TNFα in chorio pathogenesis[22,23,26-30], and because

226   scRNAseq analyses revealed gene signatures consistent with IL-1 and TNFα signaling in

227   both the monocyte/macrophage and neutrophil lung populations of IA LPS animals, we

228   blocked IL-1 signaling with the IL-1RA and TNFα with the blocking anti-TNF Ab

229   Adalimumab, administered both subcutaneous and IA to the pregnant dams. We also

230   tested their combined effect (see Fig. S9 for experimental scheme). Both reagents had

231   previously been shown to be efficacious in macaques[22,23,35].

232   Cytokine levels in the AW were only partially diminished with any of the treatments (Table

233   S2). This modest effect was confirmed by the fact that cytokine mRNA expression in the

234   lung was also minimally decreased in all the treatment groups (Table S3). LPS-induced

235   histological changes (cell infiltration and lung interstitium thickening) remained present in

236   animals given IL-1RA or anti-TNF, although lung interstitium thickening was partially

237   decreased in animals given both inhibitors (Fig. 6A).

238   Infiltration of myeloid cells into the lung was not blunted by any of the treatments, as

239   shown by both scRNAseq and flow cytometry analyses (Fig. 6B-C). Neutrophil

240   accumulation in the AW was also not blunted (p>0.9, Kruskal-Wallis tests). Similar

241   monocyte/macrophage populations were present in the lung of treated animals as in IA

242   LPS animals (Fig. 7A). However, the blockades partially suppressed some of the

243   biological processes activated by IA LPS (Fig. 7B and S10A-C). Notably, there was a

244   downward trend of the expression of genes associated with the TLR, IL-1, and TNFα

245   signaling pathways in the alveolar and interstitial macrophages, which appeared most

246   marked in the animals that had received the combined treatment (Fig. 7B). Blockades

247   also decreased the expression of genes associated with cell migration and apoptotic

248   signaling in these cells (Fig. S10A-B). However, the blockades did not blunt these

249   processes in the inflammatory monocytes (Fig. 7B and S10C).

250   Neutrophil migration into the lung was also not diminished by any of the blockades (Fig.

251   8A). As in the inflammatory monocytes, the blocking treatments did not markedly alter the

252   neutrophilic transcriptome (Fig. 8B and S10D).

253   Blockades lead to a decreased frequency of the mDC population, decreasing it below that

254   present in the control animals (Fig. S11). mDC activation, as evidenced by high HLA-DR

255   MFI, was diminished by the treatments (Fig. S11). In that case, the strongest effect was

256   seen in animals that received IL-1RA, alone or in combination (Fig. S11).

Discussion

Premature infants exposed to IUI are at increased risk of developing pulmonary and intestinal morbidities after birth [9,36,37]. Herein, we applied several complementary techniques to obtain a comprehensive view of the fetal mucosal immune response to IUI in the highly relevant Rhesus macaque model.

In this model, shortly after IA LPS, robust inflammation developed in the fetal lungs, characterized by the accumulation of immune cells into the lung and increased levels of many inflammatory mediators both in the lung tissue and the AW, similar to what had previously been described in other IUI animal models [10,11,28,29]. Myeloid cells were particularly involved, as the major cellular change occurring in the lungs of IA LPS-exposed fetuses was the massive accrual of neutrophils and inflammatory monocytes, which were absent in the control lungs. In addition, resident myeloid cells, both the alveolar and interstitial macrophages and the resident myeloid DCs, exhibited many signs of activation. Notably, scRNAseq analyses identified that response to pro-inflammatory cytokines, such as IL-1 and TNF, or to TLR, were activated in these subsets. Many of the activated biological processes were shared by the monocyte/macrophage and neutrophil populations, highlighting a general inflammatory transcriptional program. Overall, these data indicate that the fetal innate immune system can rapidly mount a strong response, a concept that remains controversial. Indeed, there have been many papers describing functional impairment in fetal/neonatal neutrophils and monocytes/macrophages as compared to their juvenile and adult counterparts (rev. in [38-40]). Described defects notably include the decreased recruitment of neutrophils and inflammatory monocytes into the lung in response to *E. coli* instillation during the same

13

280   time period, compared to juvenile mice [41]. In contrast, our data in a NHP model argue that

281   fetal neutrophils and inflammatory monocytes can quickly migrate into the pulmonary

282   environment, as these two populations became very abundant in the lung 16hrs after IA

283   LPS. Neutrophils appeared to localize in the lung in the form of aggregates, a pattern

284   reminiscent of that described in murine models of acute lung injury [42,43]. Similarly, other

285   groups had described rapid recruitment of neutrophils in fetal sheep or rhesus macaque

286   lungs in response to IA LPS or IL-1β [27,28]. It is also to be noted that the concept of

287   defective functionality of innate immune cells in human neonates mainly arises from

288   studying *in vitro* stimulated cord blood cells. It is therefore possible that these assays do

289   not fully reveal their potential. Another caveat to remember when interpreting data about

290   preterm babies' immune cell functions, is that many of these infants had just been given

291   steroids, which affect various cell type functionality. We did not administer steroids in our

292   studies, which may have allowed us to observe such robust immune responses.

293   Until recently, circulating and tissue neutrophils were considered as a homogeneous

294   population with a defined array of functions. This concept has been challenged by many

295   studies that revealed a high degree of variety in this population (rev. in [44-49]). Two main

296   mechanisms appear to drive this diversity, an intrinsic heterogeneity already initiated in

297   bone marrow precursors on one hand, and on the other hand a highly dynamic

298   transcriptional and epigenetic program triggered by exposure to the environment, notably

299   in inflammatory conditions. Our pseudo-time analyses concur with the concept of

300   functional heterogeneity, as they show several gene expression profiles within the

301   neutrophils recruited to the lungs of IA LPS exposed animals. For example, genes related

302   to granule content (*CAMP, LCN2*) or antimicrobial defense (*S100A8, S100A9*) were in

14

303   general not simultaneously expressed along inflammatory mediators (*IL1A, IL1B, CCL2,*

304   *CCL20*). Interestingly, *Bcl2A1*, a major pro-survival factor for neutrophils [50], including for

305   LPS-activated neutrophils in the Rhesus chorio-decidua [22], was also heterogeneously

306   expressed among the lung neutrophils in LPS-exposed animals, suggesting that

307   differential survival may affect neutrophil heterogeneity.   Future studies will be needed

308   to further characterize at the protein level neutrophil heterogeneity and its impact on fetal

309   responses to IUI.

310   We were also able to evaluate the role played by IL-1 or TNFα in fetal mucosal responses

311   to IA LPS. Our data show that blocking either or both of these pathways had only a partial

312   effect on lung inflammation, a finding consistent with the fact that fetal responses were

313   likely driven by both direct activation by LPS and indirect cytokine-mediated pathways.

314   The partial amelioration of disease by IL-1RA is similar to what has been previously

315   described in other IUI models [22,23,28,30], while this was, to our knowledge, the first attempt

316   at evaluating the effect of anti-TNF alone or in combination with IL-1RA. In general, the

317   anti-TNF Ab appeared to have broader effectiveness than IL-1RA, which may be due to

318   the fact that this treatment decreased levels of IL-1β expression in the lung tissue and

319   AW, whereas IL-1RA did not affect TNFα levels (Tables S2-S3).   Interestingly, the

320   combination of both blockades did not radically ameliorate the effectiveness, which

321   suggests that the two pathways are inter-connected, and that other mediators control the

322   recruitment of myeloid cells into the lung. Notably, levels of CCL2, which regulates many

323   aspects of monocyte biology, including recruitment, activation, and survival (rev. in [51]),

324   remained elevated in the lung tissue and AW of treated animals. Lung expression of

325   CXCL12, which plays a role in myeloid cell recruitment during lung injury [52,53], might also

326   be involved. Our data also show that high levels of IL-8 persisted in the lung and AW

327   despite the blockades (Tables S2 and S3). Furthermore, many neutrophilic

328   chemoattractant molecules, including chemotactic lipids, formyl peptides, and

329   complement anaphylatoxins are also released during inflammation (rev. in [54]). We did not

330   quantify these mediators in fetal lungs or AW, but because they are released through both

331   TLR and cytokine-mediated mechanisms, it is likely that they were still released despite

332   the blockades. Interestingly, compared to the fetal lung, myeloid cell recruitment in the

333   placenta was significantly reduced in the presence of either IL-1RA or anti-TNF [22,35],

334   suggesting that the mechanisms controlling cellular migration might be tissue specific.

335   Alternatively, and not exclusively, the fact that cells recruited in the placenta have a

336   maternal origin, in contrast to fetal cells migrating to the lungs, may also have driven some

337   of these differences.

338   Overall, our work in a model that phenocopies the main features of human IUI gives novel

339   insights into the inflammation rapidly developing in the fetal lung following such exposure.

340   One important conclusion from our new data is that the fetal immune system is highly

341   responsive to its environment. In this model of acute sterile inflammation, we saw that

342   fetal myeloid cells could be rapidly mobilized, migrating to the inflamed environment and

343   displaying profiles of activation very similar to those described in adult cells. This confirms

344   the new paradigm in the field of neonatal immunology, e.g., that fetuses have the capacity

345   to mount a very robust innate immune response. Our data also emphasize the fact that

346   the fetal lung is particularly responsive, as it is in close contact with the amniotic fluid,

347   whereas the fetal gut appears less affected. This study thus provides more insights into

348   why the most solid associations found between IUI exposure and post-natal morbidities

349   in humans involved mainly the lung (bronchopulmonary dysplasia, wheeziness, and

350   asthma). Our data also show that the multi-parametric mucosal inflammation that

351   develops in IUI-exposed fetuses is not easily controlled by blocking only one, or two

352   inflammatory mediators, emphasizing the need for additional mechanistic studies to better

353   understand the dynamic and complex responses that IUI triggers in exposed fetuses.

354

355

356

357

358

359

360

361

362

363

364

365

366

Materials and Methods.

Animals.

The Institutional Animal Care and Use Committee at the University of California, Davis approved all animal procedures. Normally cycling, adult female Rhesus macaques (*Macaca mulatta*) were time mated. At approximately 130 days of gestation (about 80% of term gestation), the pregnant dams received either 1 ml saline solution or 1mg of LPS (Sigma-Aldrich, St. Louis MO) in 1 ml saline solution by ultrasound guided IA injection. IA administration of LPS or saline was performed in mothers of similar weights and ages with fetus with similar fetal genders and gestational ages (Table S1). Fetuses were surgically delivered 16, 48 or 120 hrs later by cesarean section. Delivered fetuses were euthanized with pentobarbital and tissues collected. There were no spontaneous deaths or preterm labor in the animals. Some pregnant dams were given, in addition to IA LPS, either the IL-1RA (Kineret® Sobi, Stockholm, Sweden), or the anti-TNF Ab Adalimubab (HUMIRA® AbbVie Chicago, IL), or both. These inhibitors were administered subcutaneously (100mg or 40mg for IL-1RA and anti-TNF respectively) 3hrs before IA LPS as well as IA (50mg or 40 mg for IL-1RA and anti-TNF respectively) 1hr before IA LPS (see scheme on Fig. S9).

Histological evaluation of fetal lung and jejunum.

Inflated lung (30cm water pressure) and jejunum tissues were fixed in 10% formalin immediately following removal. After a series of alcohol and xylene washes, tissues were blocked in paraffin. Paraffin sections were stained with hematoxylin & eosin (H&E). 20x images were taken with a Nikon 90i Upright Widefield Microscope (Nikon Instruments

389   Inc., Melville, NY). 100μm scale bar added using Nikon Elements Software (Nikon

390   Instruments Inc., Melville, NY).

391   **Immunofluorescence staining of neutrophils and confocal analysis.**

392   Upper left lung lobe sections (5μm thick) were blocked with 4 % goat serum in PBS, and

393   then incubated 1hr at room temperature with the primary mouse-anti-human Ab diluted in

394   4% goat serum in PBS. Cross-reactivity of all Ab with Rhesus macaque cells was verified

395   on adult tissues prior to their utilization to stain fetal cells. Ab were titrated for optimal

396   detection of positive populations and MFI. Sections stained with unlabeled Ab were

397   stained with a corresponding secondary goat-anti-mouse Ab conjugated with either Alexa

398   Fluor 594, Alexa Fluor 488 or FITC (Life Technologies, dilution 1:400) for 1hr. As negative

399   control, tissues were also stained with the secondary Ab only. Sections were washed and

400   incubated with Vecta shield autofluorescence reduction kit and mounted with mounting

401   media containing DAPI (Vector Laboratories). Images were acquired using an inverted

402   microscope (Ti-E; Nikon, Japan) outfitted with a confocal scan-head (A1R; Nikon; Japan)

403   at the CCHMC Confocal Imaging Core. Analyses involving deconvolution and background

404   reduction were done with Nikon Elements Software.

405   Since neutrophils in the sections were mostly in clumps/aggregates, we evaluated the

406   number of neutrophil aggregates in 10 fields per animal. The neutrophils were identified

407   as S100A8-FITC (CF-145) and TNFAIP6-AF594 (polyclonal) (both ThermoFisher

408   Waltham, MA) double positive cells. The average area covered by neutrophils clumps

409   were also determined and normalized to the total DAPI area of the image per field. CD68-

410   FITC (KP1) (Alligent Dako, Santa Clara, CA) and HLADR-AF594 (L243) (BioLegend, San

411   Diego, CA) were also used to quantify neutrophils.

Alveolar wash analyses.

Alveolar wash was collected from the left lung. Supernatant was collected and frozen until cytokine analyses, using the NHP multiplex kit according to the manufacturer's protocol (Millipore Austin, TX). Cell pellets was cytospun and slides were stained with Diff quick. 5 fields/slide (100 cells/field) were counted twice.

Quantitative RT-PCR analyses of mucosal tissues.

From frozen lung and jejunum tissue, total RNA was extracted after homogenizing in TRIzol (Invitrogen, Carlsbad, CA). A Nanodrop spectrophotometer (Thermo Fisher Scientific) was used to measure RNA concentration and quality. 1µg of RNA was used to generate cDNA using the Verso cDNA synthesis kit (Thermo Fisher Scientific), following the manufacturer's protocol. Quantitative RT-PCR was done with a StepOnePlus real-time PCR system and rhesus specific TaqMan gene expression primers (Life Technologies, Carlsbad, CA). Eukaryotic 18S rRNA was the endogenous control used for normalization of the target RNAs. The mRNA fold change was calculated relative to the average value of the control group.

Fetal lung cell isolation.

The fetal lung was removed, and left lobe was processed into single cell suspensions as described previously [55]. The large airways were removed and approximately ~500mg of airway free tissue was collected in a gentleMACS C-tube (Miltenyi Biotec, Auburn, CA) and 5mL digest buffer was added and placed on a gentleMACS octo dissociator for programmed runs. Following dissociation, the cell suspension was passed through a 100µm filter and washed with PBS. After washing, cells underwent red cell lysis

20

434   (eBioscience, San Diego, CA) along with another pass through a 40um filter after

435   neutralization.

436   **Single cell sequencing of fetal lung cells.**

437   scRNA-seq analyses were done in a subset of animals (Table S4). ~50,000 cells per lung

438   were submitted for single cell sequencing at the Cincinnati Children's Hospital Medical

439   Center DNA Sequencing and Genotyping Core. Approximately ~16,000 cells were loaded

440   into one channel of the Chromium system using the 3 prime v3 single cell reagent kit (10X

441   Genomics, Pleasanton, CA). Following capture and lysis, cDNA was synthesized and

442   amplified as per the manufacturer's protocol (10X Genomics). The amplified cDNA was

443   used to construct Illumina sequencing libraries that were each sequenced using an

444   Illumina HiSeq 4000 machine. Raw sequencing data was processed aligned to the

445   Rhesus macaque reference Mmul_8.0.1 (Ensembl version 91) with Cell Ranger 3.0.2

446   (10X Genomics) generating expression count matrix files.

447   After doublet removal with the software DoubletFinder (version 2.0), an integrated

448   analysis was performed using R (version 3.6.3) and the Seurat package (version 3.1.0,

449   https://satijalab.org/seurat/), to identify common cell types across different experimental

450   conditions. Specifically, cells with 25% or more mitochondrial transcripts were removed,

451   as well as cells expressing fewer than 150 or more than 5000 features. After log-

452   normalization, 5000 highly variable features were identified per sample using the vst

453   method. Integration was performed using the Seurat FindIntegrationAnchors and

454   IntegrateData functions with default parameter values. The integrated data was scaled,

455   including regressing out mitochondrial percentage and cell cycle variables, followed by

21

456 application of PCA reduction. A UMAP projection was estimated based on the PCA

457 reduction and the correlation metric. Clustering of cells was done using the Seurat

458 functions FindNeighbors (based on first 30 PCs) and FindClusters (resolution=4). This

459 high-resolution was initially used to define highly discrete immune populations, with the

460 final populations subsequently aggregated into broader, higher confidence cell-types

461 based common marker genes expressed and corresponding UMAP embeddings. To

462 annotate these cell-populations, were performed a gene-set enrichment analysis on the

463 aggregated cell populations used established human and mouse cell-population marker

464 genes annotated by LungMAP, from the AltAnalyze and ToppCell databases. Immune

465 cell population labels were further evidenced using label transfer with the software

466 cellHarmony against a recently described reference human lung datasets[56,57]. Clusters

467 were orthogonally validated using the software ICGS2 in AltAnalyze, which does not

468 require a resolution setting, to confirm their presence. Identified immune cell clusters were

469 subset into a new Seurat object and re-clustered. For further analyses, Y-chromosomal

470 genes were removed from the dataset because both IA LPS-exposed fetuses were male

471 whereas animals of both sexes were present in the other experimental groups.

472 Additionally, we checked for the expression of genes *XIST* and *TSIX*, which did not

473 appear in our dataset and seem to not be drivers of differences observed. All identified

474 cell populations were required to have unique reported marker genes to ensure they were

475 not artifacts of "over-clustering". Differential gene expression analysis was performed as

476 implemented in Seurat. Plots were generated using the ggplot2 package (version 3.3.2).

477 Differentially expressed genes (DEGs) between control and LPS in the

478 monocyte/macrophage cluster with a fold change (FC) of ≥ 1.2 and adjusted p-value of ≤

22

479   0.05 were used for functional enrichment analysis of biological processes and pathways

480   using the ToppFun web portal[58]. Terms with higher expression in LPS are represented

481   as positive log p-values. Scaled expression of genes for upregulated biological processes

482   terms in the monocyte/macrophage cluster were used to plot parallel coordinate plots

483   using the ggplot2 package.

484   Differential gene expression analysis was not feasible for the neutrophil or inflammatory

485   monocyte clusters since those cells were not present in control samples (<20 cells). We

486   thus performed single sample gene set enrichment analysis (ssGSEA) in R using the

487   ssgsea2.0 package (github.com/broadinstitute/ssGSEA2.0) in order to identify enriched

488   gene ontology (GO) gene sets (MSigDB v7.0). Expression values of overlapping genes

489   of the most significant and relevant gene sets were plotted as parallel coordinate plots

490   using ggplot2.

491   In order to assess possibly different states of gene expression within neutrophils after

492   LPS exposure, single-cell trajectory analysis was performed with Monocle3 (version

493   0.2.3.0). Spatial autocorrelation analysis as implemented in Monocle3 was used to

494   determine genes that most strongly vary along the pseudo-time trajectory. The Monocle

495   algorithm is capable of ordering cells based on their transcriptomic profile in an

496   unsupervised manner and thus arrange cells along a directional path. The order of the

497   cells along this path represents different transcriptomic states within a biological process

498   even if cells are obtained at only one time point during an experiment. The scRNA-seq

499   data have been deposited in the Gene Expression Omnibus (GSE169390, reviewer

500   token:qxatqgkyhxyrhkl).

23

Flow Cytometry.

501

502 A cocktail of conjugated Ab was used to phenotype lung cell suspensions for multi-

503 parameter flow-cytometry. The following Ab were used: HLA-DR (L243), CD11c (3.9)

504 (BioLegend, San Diego, CA); CD3 (GHI/61), CD3 (SP34-2), CD19 (SJ25C1), CD20

505 (2H7), CD123 (7G3), CD45 (DO58-1283) (BD Biosciences, San Jose, CA); CD8α (RPA-

506 T8), FoxP3 (PCH101), LIVE/DEAD Fixable Aqua dead cell stain, (eBioscience, San

507 Diego, CA), CD88 (P12/1) (Bio-rad, Hercules, CA). Lung cell suspensions were treated

508 with human IgG to block Fc-receptors and stained for surface markers. Cells were then

509 washed and treated with fixation/permeabilization buffer (ThermoFisher). Following

510 permeabilization, cells were stained for intracellular markers, washed, and resuspended

511 in PBS. Cells were collected on a FACS Fortessa (BD Bioscience San Jose, CA). BD

512 FACSDiva Software v8.0.1 (BD Bioscience San Jose, CA) was used for analysis.

Statistical analyses.

513

514 GraphPad Prism 8 (GraphPad Software, La Jolla, California, USA) was used to graph

515 and analyze data for statistical significance. Data were first checked for normality and

516 values expressed as either mean ±SEM or median and interquartile range. Statistical

517 differences between 2 groups were analyzed using Mann-Whitney U-tests or Student's t-

518 test. For comparison of more than two groups, Kruskal-Wallis or One-way ANOVA were

519 used. Results were considered significantly different for p values ≤0.05. However, due to

520 the limited number of samples in some groups, we also report trends (p values between

521 0.05 and 0.1).

Author contributions.

522

24

523   C.A.C, A.H.J., H.D., S.G.K., L.A.M., I.P.J. and W.J.Z. conceived the study. C.M.J., S.M.,

524   P.P., T.I., P.S., M.C., M.D. and J.G. all performed experiments and data analysis. N.S.

525   and K.C. did the initial pre-processing of scRNAseq 10X files. All authors critically

526   reviewed the manuscript and approved the final version.

537

538

539

540

541

542

References

1   Goldenberg, R. L., Culhane, J. F., Iams, J. D. & Romero, R. Epidemiology and causes of preterm birth. *The Lancet* **371**, 75-84, doi:10.1016/S0140-6736(08)60074-4 (2008).

2   Kim, C. J. *et al.* Acute chorioamnionitis and funisitis: definition, pathologic features, and clinical significance. *Am J Obstet Gynecol* **213**, S29-S52, doi:10.1016/j.ajog.2015.08.040 (2015).

3   Saji, F. *et al.* Cytokine production in chorioamnionitis. *Journal of Reproductive Immunology* **47**, 185-196, doi:https://doi.org/10.1016/S0165-0378(00)00064-4 (2000).

4   Revello, R., Alcaide, M. J., Dudzik, D., Abehsera, D. & Bartha, J. L. Differential amniotic fluid cytokine profile in women with chorioamnionitis with and without funisitis. *The Journal of Maternal-Fetal & Neonatal Medicine* **29**, 2161-2165, doi:10.3109/14767058.2015.1077512 (2016).

5   Gomez, R. *et al.* The fetal inflammatory response syndrome. *American Journal of Obstetrics & Gynecology* **179**, 194-202, doi:10.1016/S0002-9378(98)70272-8 (1998).

6   Gitlin, D., Kumate, J., Morales, C., Noriega, L. & Arévalo, N. The turnover of amniotic fluid protein in the human conceptus. *American Journal of Obstetrics & Gynecology* **113**, 632-645, doi:10.1016/0002-9378(72)90632-1 (1972).

7   ROSS, M. G. & NIJLAND, M. J. M. Fetal Swallowing: Relation to Amniotic Fluid Regulation. *Clinical Obstetrics and Gynecology* **40**, 352-365 (1997).

8   Jobe, A. H. Effects of chorioamnionitis on the fetal lung. *Clin Perinatol* **39**, 441-457, doi:10.1016/j.clp.2012.06.010 (2012).

9   Been, J. V., Lievense, S., Zimmermann, L. J. I., Kramer, B. W. & Wolfs, T. G. A. M. Chorioamnionitis as a Risk Factor for Necrotizing Enterocolitis: A Systematic Review and Meta-Analysis. *The Journal of Pediatrics* **162**, 236-242.e232, doi:10.1016/j.jpeds.2012.07.012 (2013).

10   Kallapur, S. G., Presicce, P., Rueda, C. M., Jobe, A. H. & Chougnet, C. A. Fetal immune response to chorioamnionitis. *Semin Reprod Med* **32**, 56-67, doi:10.1055/s-0033-1361823 (2014).

11   Kallapur, S. G., Willet, K. E., Jobe, A. H., Ikegami, M. & Bachurski, C. J. Intra-amniotic endotoxin: chorioamnionitis precedes lung maturation in preterm lambs. *American Journal of Physiology-Lung Cellular and Molecular Physiology* **280**, L527-L536, doi:10.1152/ajplung.2001.280.3.L527 (2001).

12   Wolfs, T. G. A. M. *et al.* Chorioamnionitis-induced fetal gut injury is mediated by direct gut exposure of inflammatory mediators or by lung inflammation. *Am J Physiol Gastrointest Liver Physiol* **306**, G382-G393, doi:10.1152/ajpgi.00260.2013 (2014).

13   Gras-Le Guen, C. *et al.* Antenatal infection in the rabbit impairs post-natal growth and lung alveolarisation. *European Respiratory Journal* **32**, 1520-1528, doi:10.1183/09031936.00023708 (2008).

14   Pan, J. *et al.* Effects and molecular mechanisms of intrauterine infection/inflammation on lung development. *Respir Res* **19**, 93-93, doi:10.1186/s12931-018-0787-y (2018).

15   Wolfs, T. G. A. M. *et al.* Endotoxin induced chorioamnionitis prevents intestinal development during gestation in fetal sheep. *PLoS One* **4**, e5837-e5837, doi:10.1371/journal.pone.0005837 (2009).

16   Wolfs, T. G. A. M. *et al.* Antenatal ureaplasma infection impairs development of the fetal ovine gut in an IL-1-dependent manner. *Mucosal Immunology* **6**, 547-556, doi:10.1038/mi.2012.97 (2013).

587   17   Wolfs, T. G. A. M. *et al.* IL-1α mediated chorioamnionitis induces depletion of FoxP3+ cells and
588   ileal inflammation in the ovine fetal gut. *PLoS One* **6**, e18355-e18355,
589   doi:10.1371/journal.pone.0018355 (2011).
590   18   Nguyen, D. N. *et al.* Prenatal Intra-Amniotic Endotoxin Induces Fetal Gut and Lung Immune
591   Responses and Postnatal Systemic Inflammation in Preterm Pigs. *The American Journal of*
592   *Pathology* **188**, 2629-2643, doi:10.1016/j.ajpath.2018.07.020 (2018).
593   19   Makori, N. *et al.* Functional and morphological development of lymphoid tissues and immune
594   regulatory and effector function in rhesus monkeys: cytokine-secreting cells, immunoglobulin-
595   secreting cells, and CD5(+) B-1 cells appear early in fetal development. *Clin Diagn Lab Immunol*
596   **10**, 140-153, doi:10.1128/cdli.10.1.140-153.2003 (2003).
597   20   Messaoudi, I., Estep, R., Robinson, B. & Wong, S. W. Nonhuman primate models of human
598   immunology. *Antioxid Redox Signal* **14**, 261-273, doi:10.1089/ars.2010.3241 (2011).
599   21   Miller, L. A., Royer, C. M., Pinkerton, K. E. & Schelegle, E. S. Nonhuman Primate Models of
600   Respiratory Disease: Past, Present, and Future. *ILAR J* **58**, 269-280, doi:10.1093/ilar/ilx030
601   (2017).
602   22   Presicce, P. *et al.* IL-1 signaling mediates intrauterine inflammation and chorio-decidua
603   neutrophil recruitment and activation. *JCI Insight* **3**, e98306, doi:10.1172/jci.insight.98306
604   (2018).
605   23   Rueda, C. M. *et al.* Lipopolysaccharide-Induced Chorioamnionitis Promotes IL-1-Dependent
606   Inflammatory FOXP3+ CD4+ T Cells in the Fetal Rhesus Macaque. *J Immunol* **196**, 3706-3715,
607   doi:10.4049/jimmunol.1502613 (2016).
608   24   Novy, M. J. *et al.* Ureaplasma parvum or Mycoplasma hominis as Sole Pathogens Cause
609   Chorioamnionitis, Preterm Delivery, and Fetal Pneumonia in Rhesus Macaques. *Reproductive*
610   *Sciences* **16**, 56-70, doi:10.1177/1933719108325508 (2009).
611   25   Døllner, H., Vatten, L., Halgunset, J., Rahimipoor, S. & Austgulen, R. Histologic chorioamnionitis
612   and umbilical serum levels of pro-inflammatory cytokines and cytokine inhibitors. *BJOG: An*
613   *International Journal of Obstetrics & Gynaecology* **109**, 534-539, doi:10.1111/j.1471-
614   0528.2002.01028.x (2002).
615   26   Sadowsky, D. W., Adams, K. M., Gravett, M. G., Witkin, S. S. & Novy, M. J. Preterm labor is
616   induced by intraamniotic infusions of interleukin-1β and tumor necrosis factor-α
617   but not by interleukin-6 or interleukin-8 in a nonhuman primate model. *American Journal of*
618   *Obstetrics & Gynecology* **195**, 1578-1589, doi:10.1016/j.ajog.2006.06.072 (2006).
619   27   Kallapur, S. G. *et al.* Intra-amniotic IL-1β induces fetal inflammation in rhesus monkeys and
620   alters the regulatory T cell/IL-17 balance. *J Immunol* **191**, 1102-1109,
621   doi:10.4049/jimmunol.1300270 (2013).
622   28   Kallapur, S. G. *et al.* IL-1 mediates pulmonary and systemic inflammatory responses to
623   chorioamnionitis induced by lipopolysaccharide. *Am J Respir Crit Care Med* **179**, 955-961,
624   doi:10.1164/rccm.200811-1728OC (2009).
625   29   Willet, K. E. *et al.* Intra-amniotic injection of IL-1 induces inflammation and maturation in fetal
626   sheep lung. *American Journal of Physiology-Lung Cellular and Molecular Physiology* **282**, L411-
627   L420, doi:10.1152/ajplung.00097.2001 (2002).
628   30   Berry, C. A. *et al.* Interleukin-1 in lipopolysaccharide induced chorioamnionitis in the fetal sheep.
629   *Reprod Sci* **18**, 1092-1102, doi:10.1177/1933719111404609 (2011).
630   31   Nikiforou, M. *et al.* Intra-amniotic Candida albicans infection induces mucosal injury and
631   inflammation in the ovine fetal intestine. *Sci Rep* **6**, 29806-29806, doi:10.1038/srep29806
632   (2016).
633   32   McGovern, N. *et al.* Human fetal dendritic cells promote prenatal T-cell immune suppression
634   through arginase-2. *Nature* **546**, 662-666, doi:10.1038/nature22795 (2017).

27

635   33   Xie, X. *et al.* Single-cell transcriptome profiling reveals neutrophil heterogeneity in homeostasis
636   and infection. *Nature Immunology* **21**, 1119-1133, doi:10.1038/s41590-020-0736-z (2020).
637   34   Evrard, M. *et al.* Developmental Analysis of Bone Marrow Neutrophils Reveals Populations
638   Specialized in Expansion, Trafficking, and Effector Functions. *Immunity* **48**, 364-379.e368,
639   doi:10.1016/j.immuni.2018.02.002 (2018).
640   35   Presicce, P. *et al.* TNF-Signaling Modulates Neutrophil-Mediated Immunity at the Feto-Maternal
641   Interface During LPS-Induced Intrauterine Inflammation. *Frontiers in Immunology* **11**,
642   doi:10.3389/fimmu.2020.00558 (2020).
643   36   Metcalfe, A., Lisonkova, S., Sabr, Y., Stritzke, A. & Joseph, K. S. Neonatal respiratory morbidity
644   following exposure to chorioamnionitis. *BMC Pediatr* **17**, 128-128, doi:10.1186/s12887-017-
645   0878-9 (2017).
646   37   Lau, J. *et al.* Chorioamnionitis with a fetal inflammatory response is associated with higher
647   neonatal mortality, morbidity, and resource use than chorioamnionitis displaying a maternal
648   inflammatory response only. *American Journal of Obstetrics & Gynecology* **193**, 708-713,
649   doi:10.1016/j.ajog.2005.01.017 (2005).
650   38   Kumar, S. K. M. & Bhat, B. V. Distinct mechanisms of the newborn innate immunity. *Immunology
651   Letters* **173**, 42-54, doi:https://doi.org/10.1016/j.imlet.2016.03.009 (2016).
652   39   Lawrence, S. M., Corriden, R. & Nizet, V. Age-Appropriate Functions and Dysfunctions of the
653   Neonatal Neutrophil. *Frontiers in Pediatrics* **5**, doi:10.3389/fped.2017.00023 (2017).
654   40   Yu, J. C. *et al.* Innate Immunity of Neonates and Infants. *Frontiers in immunology* **9**, 1759-1759,
655   doi:10.3389/fimmu.2018.01759 (2018).
656   41   McGrath-Morrow, S. A. *et al.* The innate immune response to lower respiratory tract E. Coli
657   infection and the role of the CCL2-CCR2 axis in neonatal mice. *Cytokine* **97**, 108-116,
658   doi:10.1016/j.cyto.2017.06.002 (2017).
659   42   Park, I. *et al.* Neutrophils disturb pulmonary microcirculation in sepsis-induced acute lung injury.
660   *Eur Respir J* **53**, 1800786, doi:10.1183/13993003.00786-2018 (2019).
661   43   Zarbock, A., Singbartl, K. & Ley, K. Complete reversal of acid-induced acute lung injury by
662   blocking of platelet-neutrophil aggregation. *J Clin Invest* **116**, 3211-3219, doi:10.1172/JCI29499
663   (2006).
664   44   Filep, J. G. & Ariel, A. Neutrophil heterogeneity and fate in inflamed tissues: implications for the
665   resolution of inflammation. *American Journal of Physiology-Cell Physiology* **319**, C510-C532,
666   doi:10.1152/ajpcell.00181.2020 (2020).
667   45   Silvestre-Roig, C., Hidalgo, A. & Soehnlein, O. Neutrophil heterogeneity: implications for
668   homeostasis and pathogenesis. *Blood* **127**, 2173-2181, doi:10.1182/blood-2016-01-688887
669   (2016).
670   46   Ng, L. G., Ostuni, R. & Hidalgo, A. Heterogeneity of neutrophils. *Nature Reviews Immunology* **19**,
671   255-265, doi:10.1038/s41577-019-0141-8 (2019).
672   47   Alder, M. N. *et al.* Olfactomedin 4 marks a subset of neutrophils in mice. *Innate Immun* **25**, 22-
673   33, doi:10.1177/1753425918817611 (2019).
674   48   Hu, N. *et al.* Coexpression of CD177 and membrane proteinase 3 on neutrophils in
675   antineutrophil cytoplasmic autoantibody–associated systemic vasculitis: Anti–proteinase 3–
676   mediated neutrophil activation is independent of the role of CD177-expressing neutrophils.
677   *Arthritis & Rheumatism* **60**, 1548-1557, doi:10.1002/art.24442 (2009).
678   49   Pillay, J. *et al.* A subset of neutrophils in human systemic inflammation inhibits T cell responses
679   through Mac-1. *J Clin Invest* **122**, 327-336, doi:10.1172/JCI57990 (2012).
680   50   Vier, J., Groth, M., Sochalska, M. & Kirschnek, S. The anti-apoptotic Bcl-2 family protein A1/Bfl-1
681   regulates neutrophil survival and homeostasis and is controlled via PI3K and JAK/STAT signaling.
682   *Cell Death Dis* **7**, e2103-e2103, doi:10.1038/cddis.2016.23 (2016).

683   51   Gschwandtner, M., Derler, R. & Midwood, K. S. More Than Just Attractive: How CCL2 Influences
684   Myeloid Cell Behavior Beyond Chemotaxis. *Frontiers in Immunology* **10**,
685   doi:10.3389/fimmu.2019.02759 (2019).
686   52   Petty, J. M. *et al.* Pulmonary Stromal-Derived Factor-1 Expression and Effect on Neutrophil
687   Recruitment during Acute Lung Injury. *The Journal of Immunology* **178**, 8148-8157,
688   doi:10.4049/jimmunol.178.12.8148 (2007).
689   53   Konrad, F. M., Meichssner, N., Bury, A., Ngamsri, K.-C. & Reutershan, J. Inhibition of SDF-1
690   receptors CXCR4 and CXCR7 attenuates acute pulmonary inflammation via the adenosine A(2B)-
691   receptor on blood cells. *Cell Death Dis* **8**, e2832-e2832, doi:10.1038/cddis.2016.482 (2017).
692   54   Metzemaekers, M., Gouwy, M. & Proost, P. Neutrophil chemoattractant receptors in health and
693   disease: double-edged swords. *Cell Mol Immunol* **17**, 433-450, doi:10.1038/s41423-020-0412-0
694   (2020).
695   55   Zacharias, W. & Morrisey, E. Isolation and culture of human alveolar epithelial progenitor cells.
696   *Protoc. Exch* (2018).
697   56   Travaglini, K. J. *et al.* A molecular cell atlas of the human lung from single-cell RNA sequencing.
698   *Nature* **587**, 619-625, doi:10.1038/s41586-020-2922-4 (2020).
699   57   DePasquale, E. A. K. *et al.* cellHarmony: cell-level matching and holistic comparison of single-cell
700   transcriptomes. *Nucleic Acids Res* **47**, e138, doi:10.1093/nar/gkz789 (2019).
701   58   Chen, J., Bardes, E. E., Aronow, B. J. & Jegga, A. G. ToppGene Suite for gene list enrichment
702   analysis and candidate gene prioritization. *Nucleic Acids Res* **37**, W305-W311,
703   doi:10.1093/nar/gkp427 (2009).

704
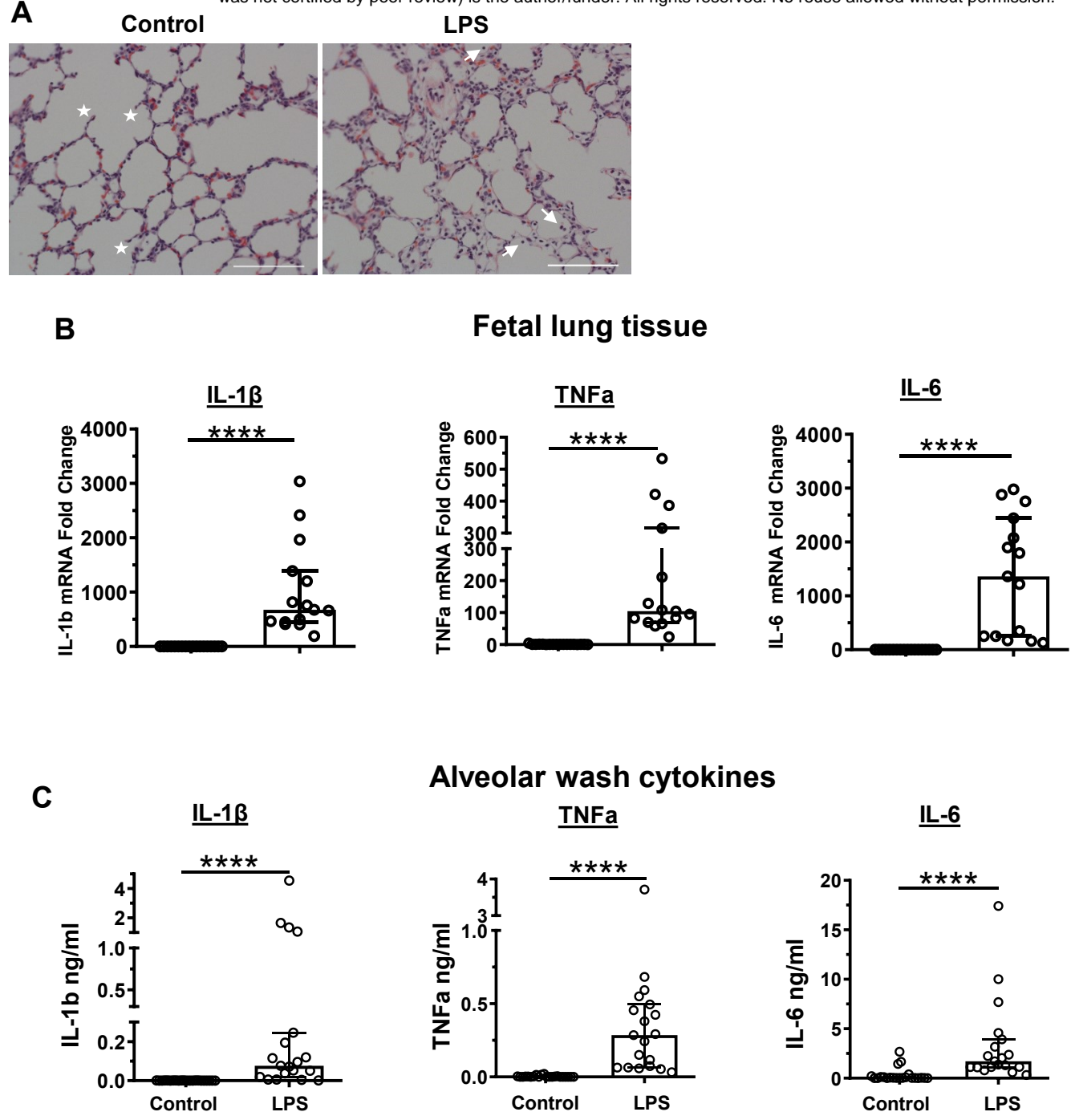
Fig. 1

Fig. 1. Fetal lung response 16 hours post IA LPS exposure. (A) 20x hematoxylin & eosin (H&E) stain of fetal lung from control and LPS exposed fetuses at 16 hours following IA LPS exposure; stars denote secondary septa, arrows represent infiltrating cells in alveolar space and scale bar is 100μm. IL-1β, TNFα, and IL-6, mRNA expression in fetal lung tissue (B) and concentration in the alveolar wash (C) in control and 16 hours post IA LPS. Data presented as median and interquartile range, Mann-Whitney U test; ****p≤0.0001.

Fig. 2

Whole Lung

A

Immune Cells Only

B   Control   LPS

C

D CD88 (C5AR1)

E   CD45$^+$%   CD88$^+$(CD45$^+$)%
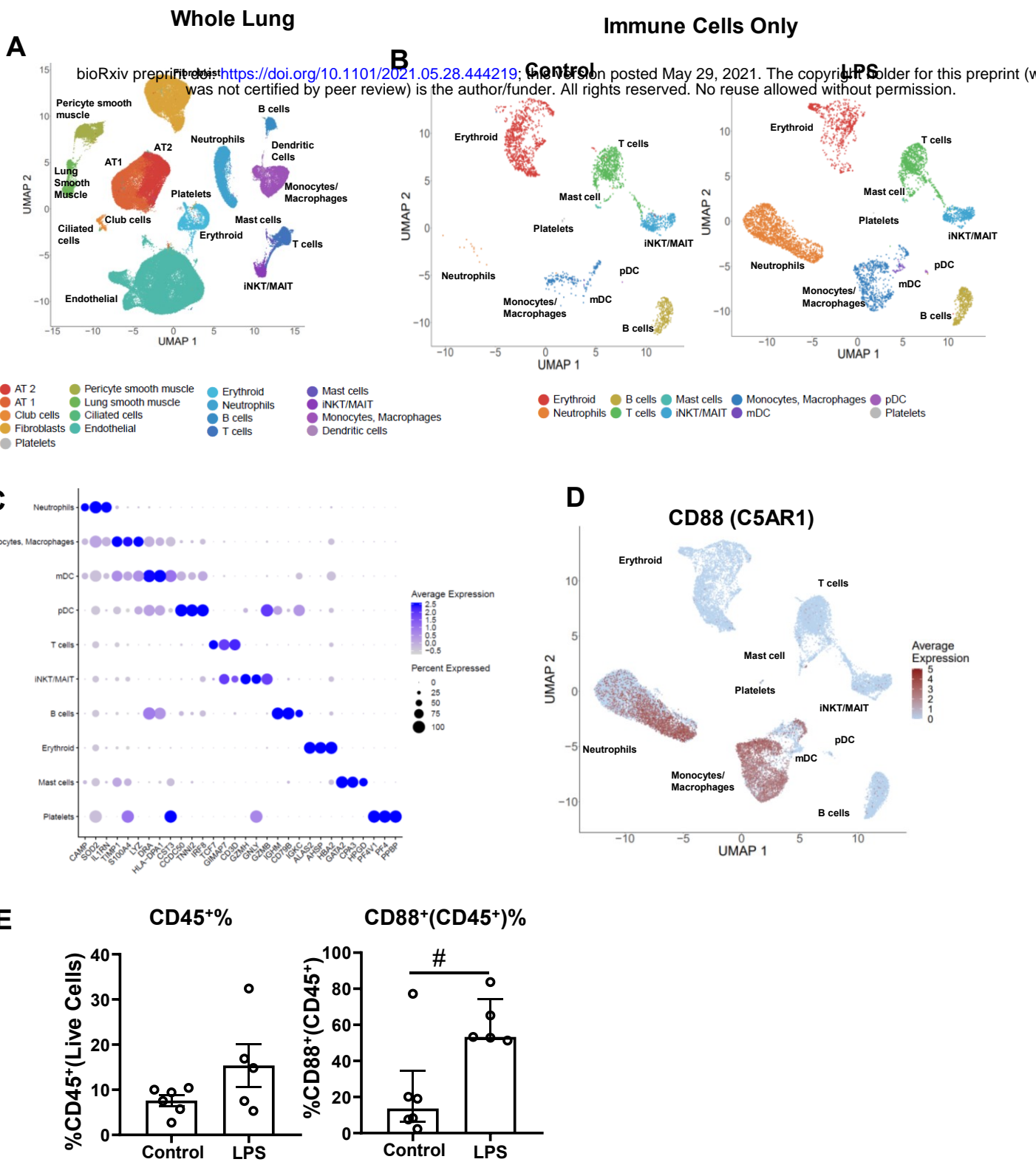
Fig. 2. Single cell RNAseq analysis of the fetal lung 16 hours post IA LPS exposure. The left lobe of fetal lung was processed into single cell suspensions and submitted for single cell sequencing. **(A)** UMAP from combined control and LPS-exposed animals (2 each). **(B)** Control (left) and IA LPS (right) exposed animals UMAP of re-clustered immune cell populations. **(C)** Representative dot plot of canonical cell type markers used in the identification of hematopoietic populations. **(D)** Feature plot of CD88(C5AR1) expression across hematopoietic cell populations and **(E)** percentage of total CD45$^+$ within live cells and CD88$^+$ within CD45$^+$ cells in lung. Data presented as mean with SEM, student's unpaired t-test (CD45$^+$%) or median and interquartile range, Mann-Whitney U test (CD88$^+$%); #0.05≥p≤0.10.

Fig. 3

A

B
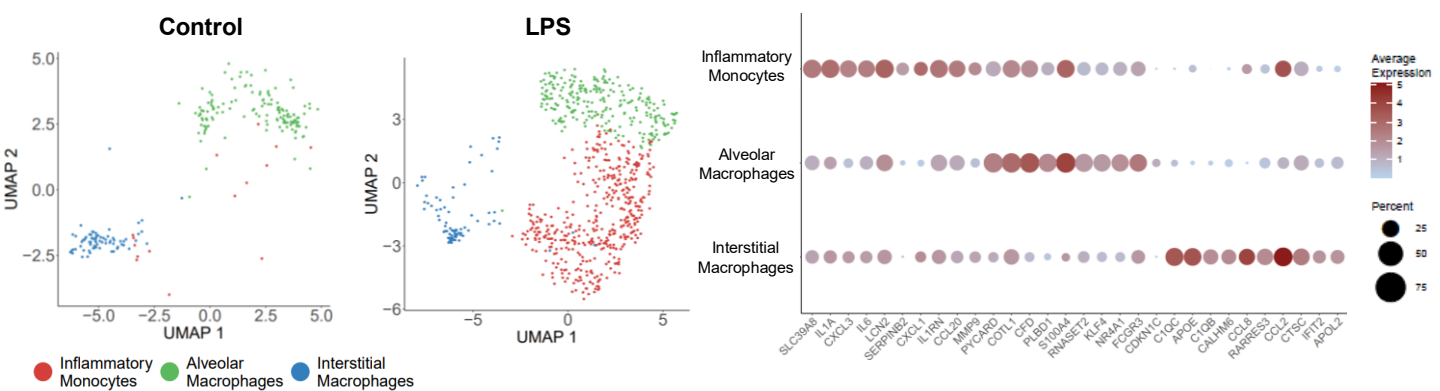
C
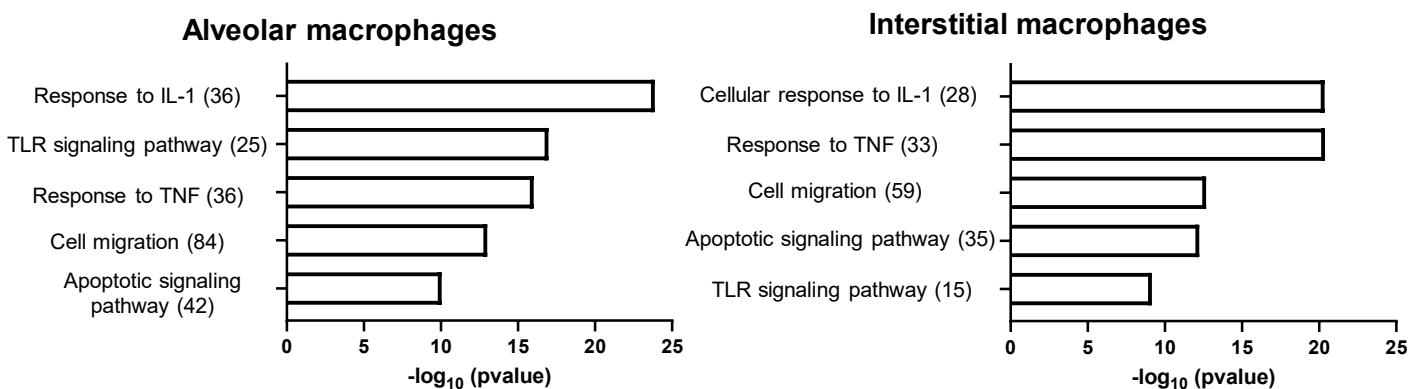
D
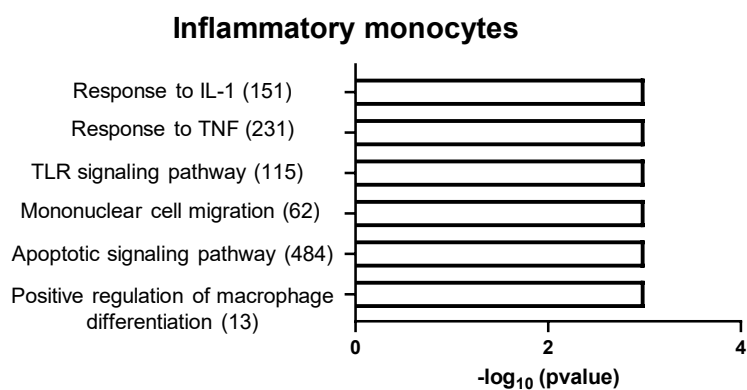
Fig. 3. Fetal lung monocyte/macrophage response to IA LPS. (A) UMAPs of fetal lung myeloid cell populations in control (left) and IA LPS (right) fetuses. **(B)** Bubble plot of the top 10 conserved genes in the inflammatory monocyte, alveolar macrophage, and interstitial macrophage populations in the fetal lung of IA LPS exposed fetuses. **(C)** Functional enrichment analysis of upregulated biological processes based on differentially expressed genes (alveolar, interstitial macrophages) using ToppFun. **(D)** ssGSEA analysis of enriched gene ontology (GO) terms in inflammatory monocytes. Numbers in parentheses represent the total number of genes for each process.

Fig. 4
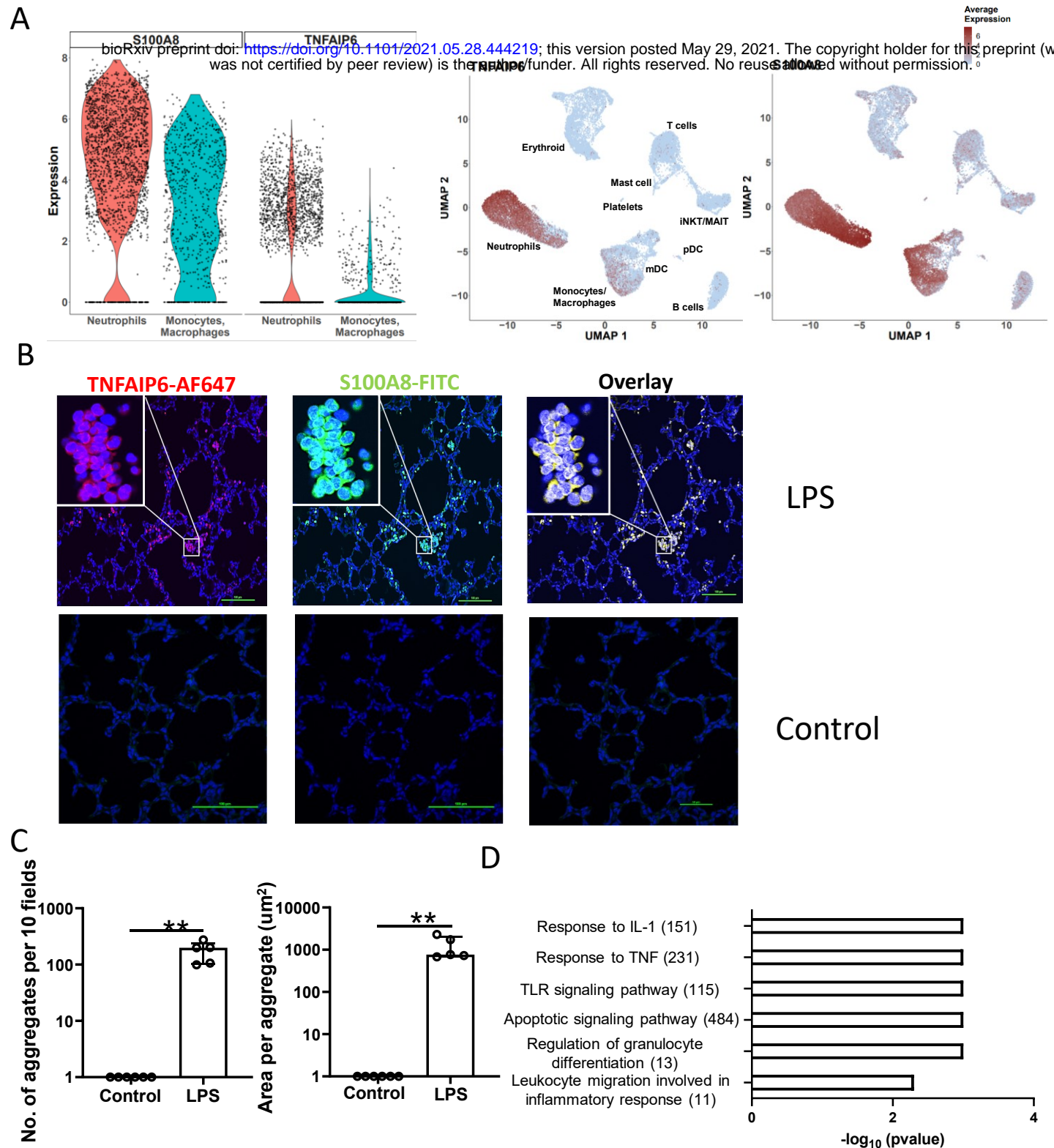
Fig. 4. Fetal lung neutrophil response to IA LPS. (A) Violin (left) and feature (right) plot of TNFIAP6 and S100A8 expression in fetal lung neutrophils and monocyte/macrophage population following IA LPS exposure. **(B)** Immunofluorescence of IA LPS exposed fetal lung stained for S100A8 and TNFAIP6; scale bar is 100μm. **(C)** Neutrophil aggregate count (left) and area (right) in the fetal lungs of control and IA LPS fetuses. Data presented as median and interquartile range, Mann-Whitney U test; **p≤0.01. **(D)** ssGSEA analysis of enriched GO terms in neutrophils. Numbers in parentheses represent the total number of genes for each process.

Fig. 5

A

B
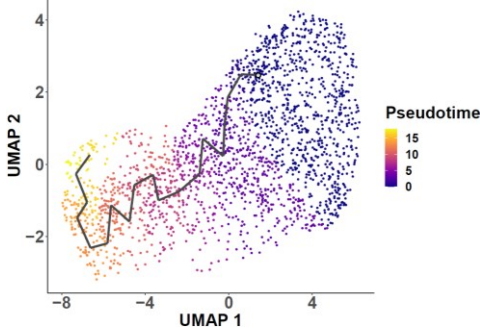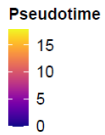
Fig. 5. Pseudo-time analysis of fetal lung neutrophil response to IA LPS. (A) Pseudo-time trajectory analysis of IA LPS exposed fetal lung neutrophils using Monocle. **(B)** Plots of genes from GO biological pathways response to IL-1 and TLR signaling pathway across pseudo-time.

Fig. 6

A

| Control	LPS	LPS+IL-1RA	LPS+aTNF	LPS+IL-1RA+aTNF

B
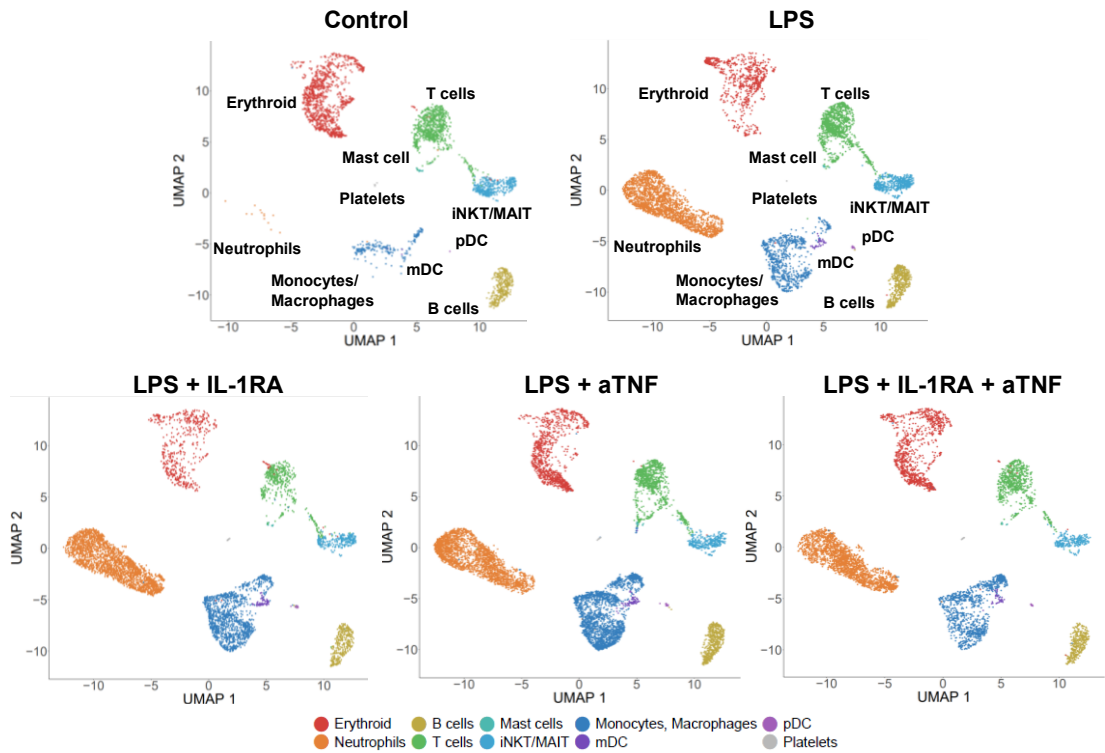
C
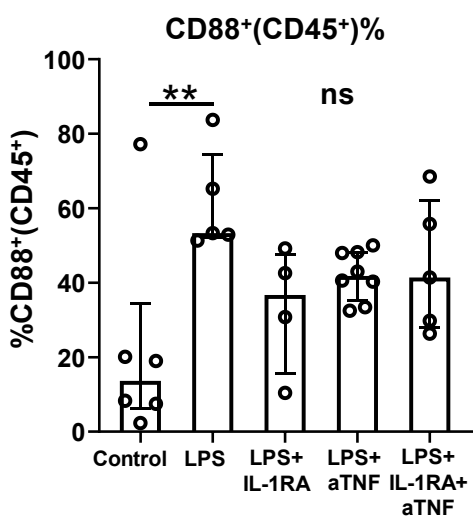
Fig. 6. Hematopoietic cell changes in the fetal lung following blocking IL-1 and TNF signaling. (A) 20x H&E sections of fetal control, lps, lps+IL-1RA, lps+anti-TNF, and lps+IL-1RA+anti-TNF exposed animals; stars denote secondary septa, arrows represent cells in alveolar space and scale bar is 100µm. **(B)** UMAPs of the hematopoietic cells from control, lps, lps+IL-1RA, lps+anti-TNF, and lps+ IL-1RA+anti-TNF exposed animals. **(C)** CD88$^+$ percentage within the CD45$^+$ cells. Data presented as median and interquartile range, Kruskai-Wallis test; **p≤0.01.
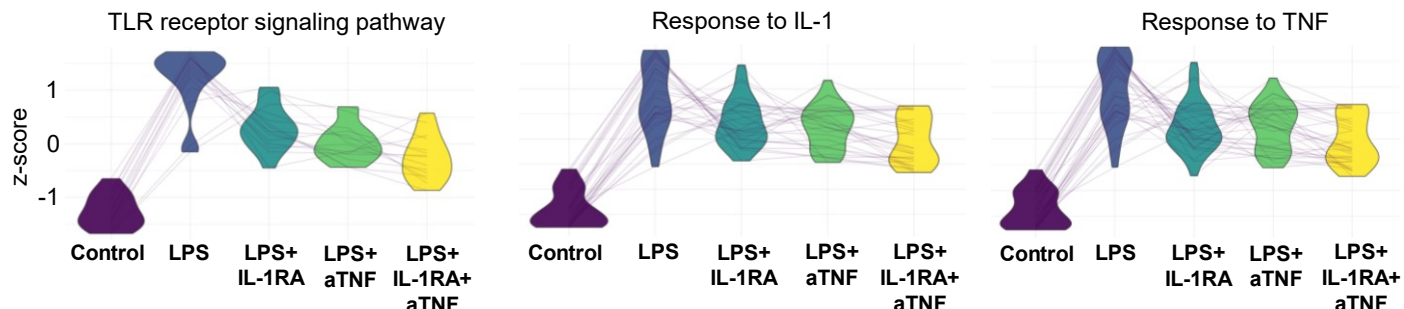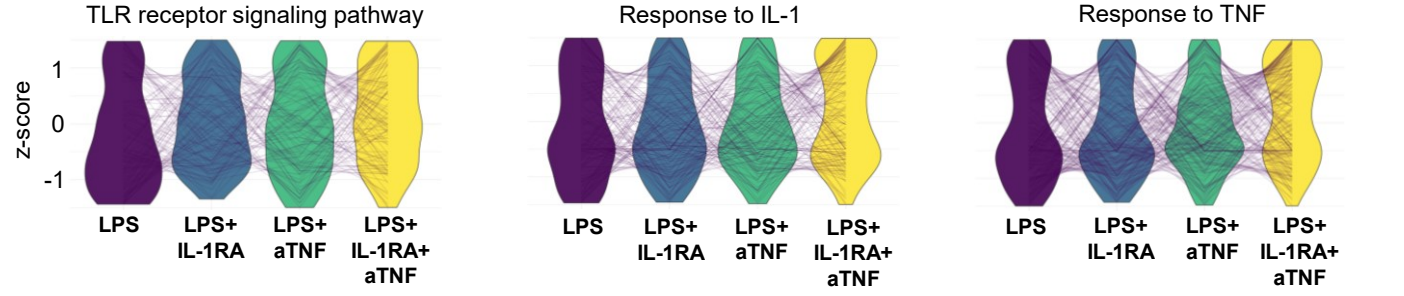
Fig. 7

A
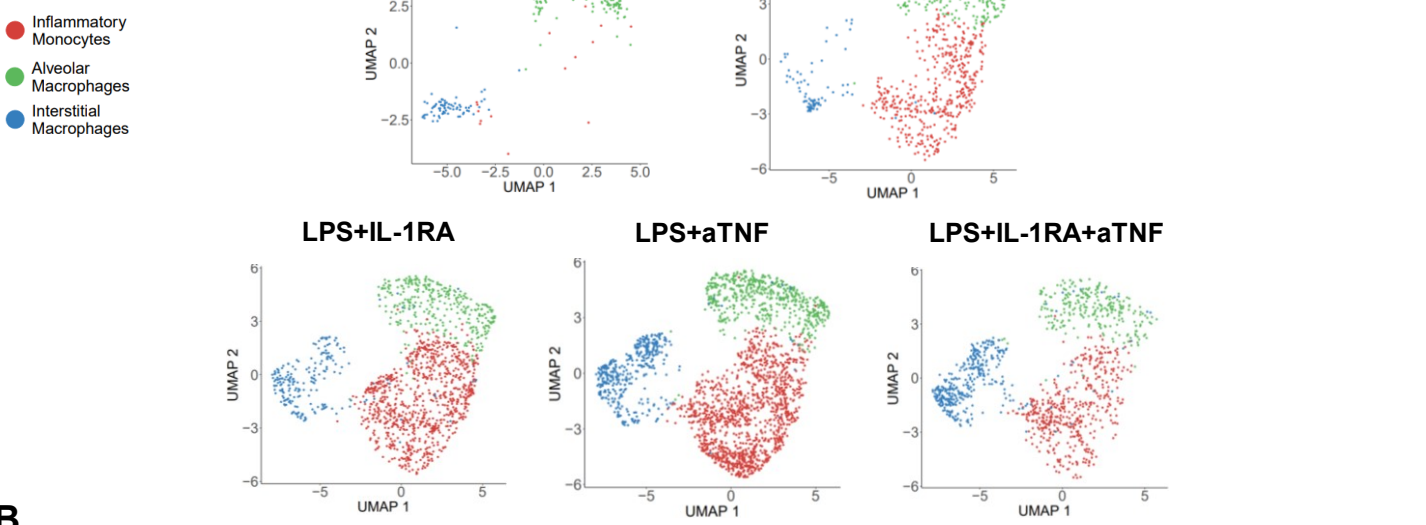
B

## Alveolar Macrophages
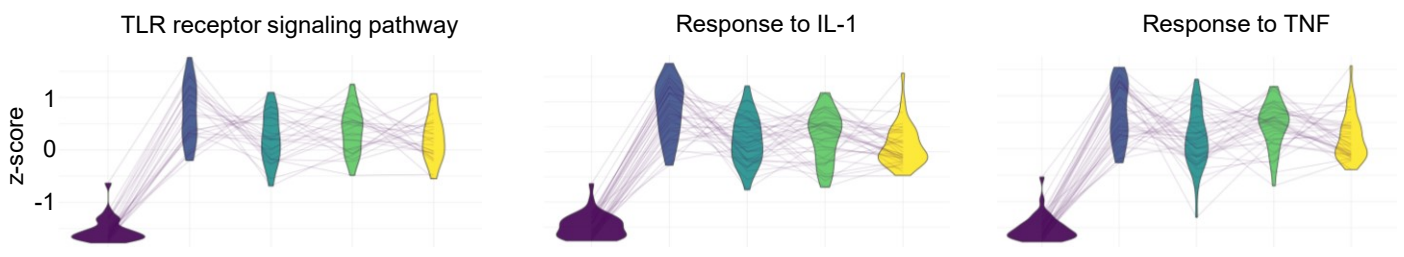
Interstitial Macrophages

Inflammatory Monocytes

Fig. 7. Fetal lung monocyte/macrophage population across treatment conditions. (A) UMAPs of fetal lung myeloid populations and **(B)** parallel coordinate plots of scaled expression of representative genes in select biological processes across treatment conditions in alveolar, interstitial macrophages and inflammatory monocytes.

Fig. 8

A

B
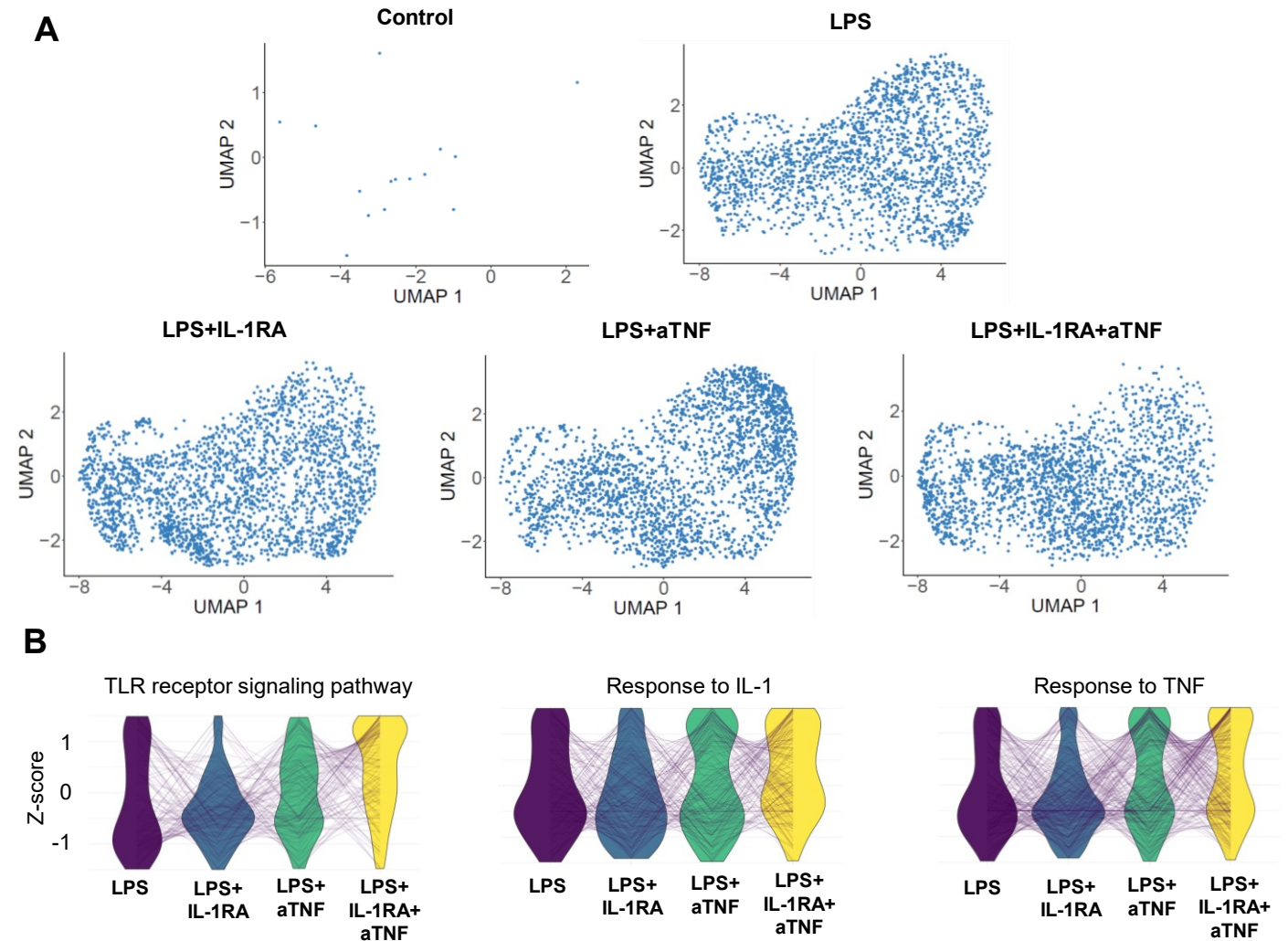
Fig. 8. Fetal lung neutrophils in response to IA LPS and blockades. (A) UMAPs of the neutrophil population across treatment conditions. **(B)** Parallel coordinate plots of scaled expression of representative genes in select biological processes across treatment conditions.